JOURNAL OF NATURAL PRODUCTS

pubs.acs.org/jnp

Article

Modulation of *in Vitro* SARS-CoV-2 Infection by *Stephania tetrandra* and Its Alkaloid Constituents

Aswad Khadilkar, Zoie L. Bunch, Jessica Wagoner, Vandana Ravindran, Jessica M. Oda, Warren S. Vidar, Trevor N. Clark, Preston K. Manwill, Daniel A. Todd, Sarah A. Barr, Lauren K. Olinger, Susan L. Fink, Wendy K. Strangman, Roger G. Linington, John B. MacMillan, Nadja B. Cech, and Stephen J. Polyak*

Cite This: *J. Nat. Prod.* 2023, 86, 1061−1073

Read Online

ACCESS | Metrics & More | Article Recommendations | Supporting Information

ABSTRACT: Botanical natural products have been widely consumed for their purported usefulness against COVID-19. Here, six botanical species from multiple sources and 173 isolated natural product compounds were screened for blockade of wild-type (WT) SARS-CoV-2 infection in human 293T epithelial cells overexpressing ACE-2 and TMPRSS2 protease (293TAT). Antiviral activity was demonstrated by an extract from *Stephania tetrandra*. Extract fractionation, liquid chromatography−mass spectrometry (LC-MS), antiviral assays, and computational analyses revealed that the alkaloid fraction and purified alkaloids tetrandrine, fangchinoline, and cepharanthine inhibited WT SARS-CoV-2 infection. The alkaloids and alkaloid fraction also inhibited the delta variant of concern but not WT SARS-CoV-2 in VeroAT cells. Membrane permeability assays demonstrate that the alkaloids are biologically available, although fangchinoline showed lower permeability than tetrandrine. At high concentrations, the extract, alkaloid fractions, and pure alkaloids induced phospholipidosis in 293TAT cells and less so in VeroAT cells. Gene expression profiling during virus infection suggested that alkaloid fraction and tetrandrine displayed similar effects on cellular gene expression and pathways, while fangchinoline showed distinct effects on cells. Our study demonstrates a multifaceted approach to systematically investigate the diverse activities conferred by complex botanical mixtures, their cell-context specificity, and their pleiotropic effects on biological systems.

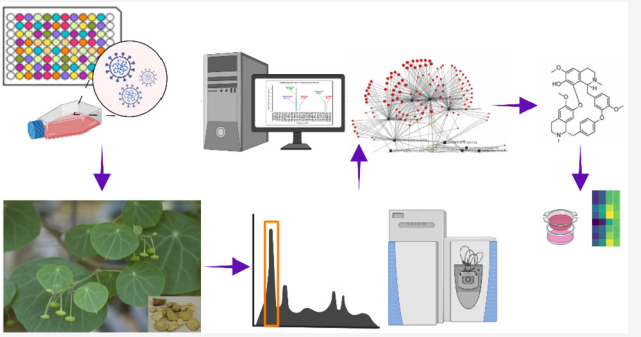

Viruses have always and will continue to plague humanity. For many viruses that cause serious illness and death, as we have experienced with the ongoing COVID-19 global pandemic, there is a dearth of effective treatments. Current single-drug antiviral countermeasures such as remdesivir (RDV), which inhibits virus replication by targeting the viral RNA dependent RNA polymerase, have limited efficacy.[1−3] In fact, the use of remdesivir in a recent Ebola outbreak in the Congo was discontinued for lack of efficacy.[4] The drug was repurposed for severe COVID-19[5] and received emergency use authorization, though subsequent studies have shown limited and variable efficacy against COVID-19.[6] Moreover, remdesivir's utility is restricted to severely ill, hospitalized patients and requires multiday intravenous administration. Remdesivir is therefore impractical for reducing viral transmission and mass prophylaxis or treatment, especially in home settings. Three years into the pandemic, molnupiravir, an orally administered inhibitor of several RNA-dependent RNA polymerases, including SARS-CoV2's,[7] has shown clinical promise,[8] as has Paxlovid, an inhibitor of the viral protease.[9] Paxlovid and molnupiravir have 89% and 30% efficacy, respectively, defined as prevention of hospitalization or death.[8,10−12] While current orally available drugs for SARS-CoV-2 are highly effective at reducing hospitalization, they are not effective for all indications (including postexposure prophylaxis). Paxlovid resistance has been described *in vitro*, and symptom rebound upon finishing a course of paxlovid has been described clinically,[13−17] similar to what has been found for remdesivir.[18−20] Moreover, pre-existing Paxlovid-resistant mutants have been found in therapy naive patients.[21,22] Thus, there is room for development of additional countermeasures that have antiviral and/or immunomodulatory properties.[23]

During the COVID-19 pandemic, increased use of botanical natural products (referred to in the US as "dietary supplements") was observed around the world.[24−26] This increased usage was driven by the belief that such products would be helpful to treat or prevent infection by the virus. The use of

Received: February 24, 2023
Published: April 12, 2023

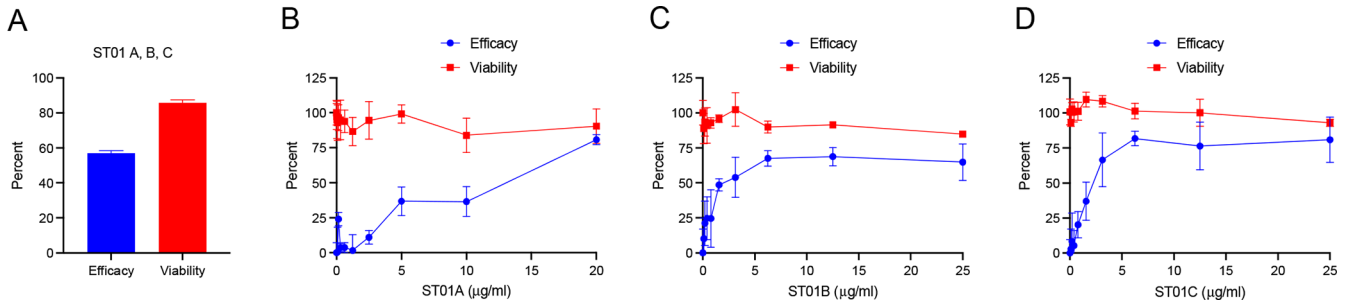

Figure 1. *Stephania tetrandra* inhibits SARS-CoV-2 infection in 293TAT cells. (A) 293TAT cells were treated with 10 μg/mL of ST01A, B, or C immediately prior to infection with SARS-CoV-2 at a multiplicity of infection (MOI) of 0.01. Parallel wells were not infected and treated with the extracts to monitor effects on cell viability. After 48 h, cell viability was assessed through measurement of cellular ATP levels. Antiviral effects were quantified in terms of efficacy, while viability reflects the effects of the extracts on cell health in noninfected cells. (B–D) Extracts' antiviral efficacy in infected cells and cell viability in noninfected cells when tested in dose–response experiments.

plant-based therapies to treat viral infections dates back thousands of years. However, in the current context, quality control of the botanical natural product industry in the US and elsewhere is stymied by lack of resources and limited information about the efficacy, active constituents, and mechanism of action of many plants with purported effectiveness. Botanical natural products are often used medicinally based on limited or anecdotal evidence and without the oversight of those knowledgeable about traditional or current therapeutic strategies. Not surprisingly, there have been cases during the pandemic where companies seeking profit have made false or fraudulent claims about the effectiveness of dietary supplements against COVID-19.[27,28] In this study, we sought to rigorously evaluate a series of botanical natural products (both complex extracts and isolated constituents) for their *in vitro* effectiveness as anti-SARS-CoV-2 agents.

Stephania tetrandra, known as FangJi (Pinyin name) in Chinese, is a medicinal plant that has been used for centuries as part of traditional Chinese medicine (TCM). Extracts from the plant have demonstrated health-promoting effects such as anti-inflammatory and anticancer effects *in vitro* and *in vivo*.[29] *S. tetrandra* is rich in alkaloids, flavonoids, and steroids. Alkaloids are the main active ingredients with more than 45 known structures. Most studied are the bisbenzylisoquinoline alkaloids including tetrandrine (**1**), fangchinoline (**2**), and cepharanthine (**3**). The extract and its alkaloid constituents are thought to confer health promotion via multiple postulated mechanisms of action.[29]

A critical challenge in botanical natural products research is that biological activity may be due to multiple compounds that may operate by multiple different mechanisms of action.[30] Recently, our groups have been engaged in the development of methodological and computational approaches that employ metabolomic and genomic data sets to assign active constituents from complex natural products and predict mechanism of action.[31−36] With this project, we sought to test these approaches with the goal of identifying botanical compounds effective against SARS-CoV-2. Herein, we describe the anti-SARS-CoV-2 and cellular effects of *S. tetrandra* extracts and isolated alkaloids from the extract. To begin to address the clinical translatability and mechanisms of action of these alkaloids, we examined their permeability across artificial membranes and determined their effects on viral and cellular RNA expression during virus infection.

RESULTS AND DISCUSSION

We prepared a custom library of 173 pure natural compounds and 60 extracts from six different botanical species (Figures S1, S2). Compounds were obtained from Chromadex and covered the chemical space typically occupied by botanicals including alkaloids, diterpene glycosides, flavonoids, phenolic acids, terpenoids, and triterpenes. Isolated compounds and extracts were prepared in 96-well plates at 10 μM or 10 mg/mL, respectively. The final library consisted of three 96-well plates (Table S1).

The 60 botanical extracts consisted of three replicate preparations of six different botanical extracts from multiple commercial and academic sources. The six extracts were from the plants *Artemisia annua* (9 extracts from 3 suppliers), *Hydrastis canadensis* L. (24 extracts from 8 suppliers), *Camellia sinensis* (L.) Kuntze (9 extracts from 3 suppliers), *Withania somnifera* (L.) Dunal (12 extracts from 4 suppliers), *Sambucus nigra* L. (3 extracts from 1 supplier), and *S. tetrandra* S. Moore (3 extracts from 1 supplier) (Figure S2). With these extracts and compounds, we sought to evaluate antiviral activity in a cell culture model.

For the initial screen, we tested at concentrations of 10 μg/mL for extracts and 10 μM for pure compounds as single biological replicates. Antiviral activity was evaluated against live SARS-CoV-2 in a biosafety level 3 (BSL3) laboratory. Parallel plates containing treated cells that were not infected with virus were processed to monitor for extract/compound-induced cellular toxicity. The antiviral assay was based on virus-induced cytopathic effect (CPE, see Experimental Section). The test cell line was HEK 293T cells that were engineered to overexpress the SARS-CoV-2 receptor angiotensin converting enzyme 2 (ACE2) and the cell surface protease transmembrane serine protease 2 (TMPRSS2).[37] We refer to these cells as 293TAT. Expression of these molecules on the surface of cells facilitates virus entry by fusion of the viral membrane with the plasma membrane of the cell.[38] Using criteria of at least 20% antiviral efficacy in virus-infected cells with less than 20% cellular toxicity on noninfected cells, the initial screen produced several hits from pure compounds including baicalin, baicalein, cinchonine, coniferaldehyde, vinpocetine, and lobeline, a hit rate of 5/173 (2.9%) (Figure S3). Positive controls on all plates included remdesivir, an approved antiviral for SARS-CoV-2 that inhibits the viral polymerase,[39] and camostat, an approved drug that inhibits TMPRSS2 and hence virus entry.[38] In Screen 1, remdesivir at 10 μM was toxic to cells, while camostat at 2.5 μM conferred

https://doi.org/10.1021/acs.jnatprod.3c00159
J. Nat. Prod. 2023, 86, 1061−1073

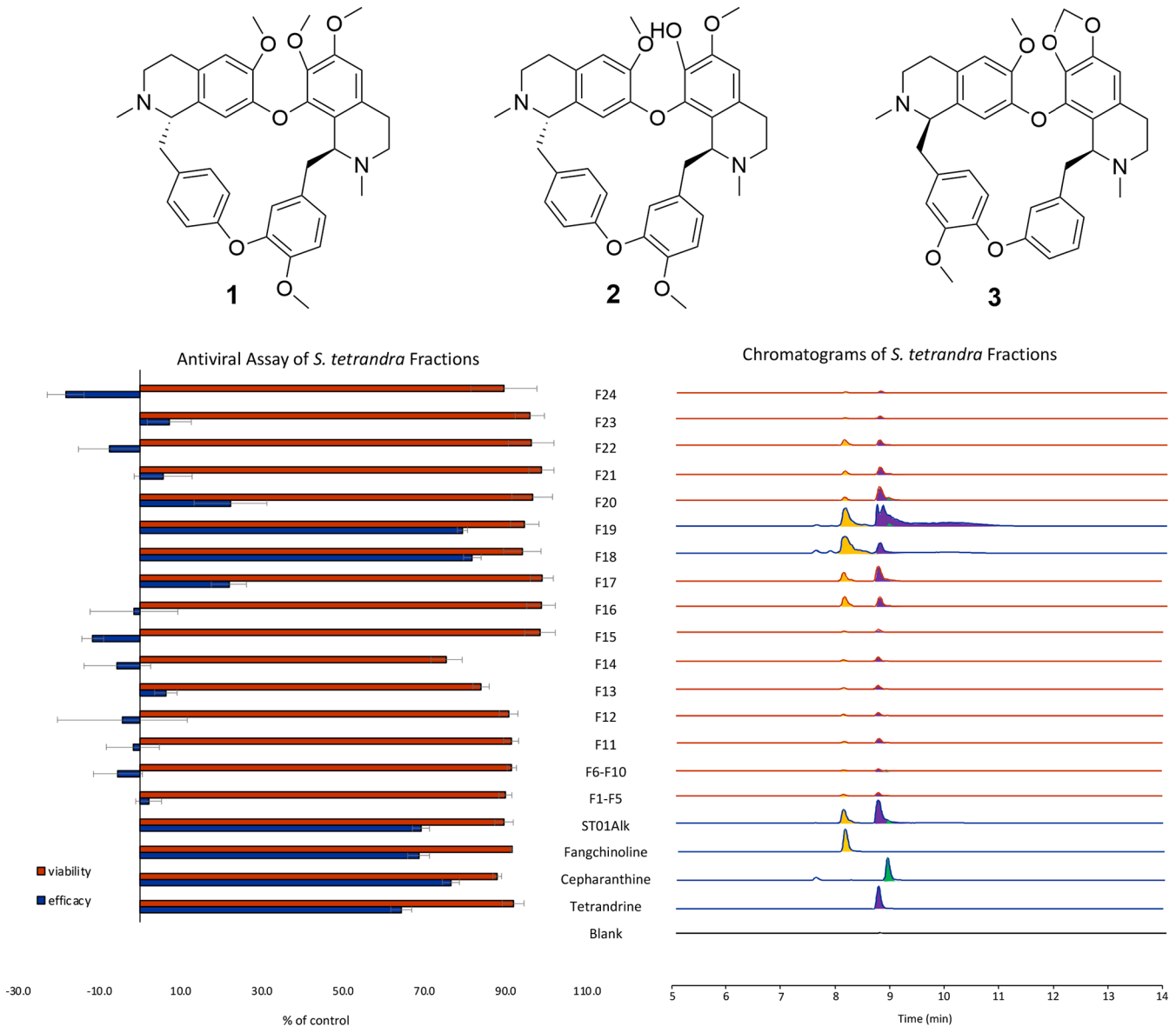

Figure 2. Antiviral activity of *S. tetrandra* fractions. Right panel: Base peak LC-MS chromatograms of the *S. tetrandra* alkaloid partition and its fractions. Selected chromatograms of the pure alkaloid standards and a base peak chromatogram of a methanol blank control are also shown. Alkaloid-rich fractions and standards are shown with blue traces. Peaks identified as fangchinoline (**2**), tetrandrine (**1**), and cepharanthine (**3**) are shaded in yellow, purple, and green, respectively. All chromatograms were normalized to a signal intensity of 8×10^9 except the fangchinoline, cepharantine, and tetrandrine standards, which were normalized to 1.0×10^9, 4.26×10^8, and 1.33×10^9, respectively. Left panel: *S. tetrandra* was fractionated as described in the Experimental Section, and an alkaloid-enriched partition (ST01Alk), bulk fractions (F1−F5 and F6−10), and individual fractions (F11−F24) were added to 293TAT cells at 1 μg/mL (extracts) or 1 μM (isolated alkaloids) immediately prior to infection with SARS-CoV-2 at a multiplicity of infection (MOI) of 0.01. Parallel wells of noninfected cells were treated with the fractions or compounds to monitor effects on cell viability. After 48 h, cell viability was assessed through measurement of cellular ATP levels. Antiviral effects were quantified in terms of efficacy, while viability reflects the effects of the extracts on cell health.

23 ± 3.2% antiviral efficacy with no cellular toxicity (Figure S3). The antiviral efficacy of baicalein was validated in dose−response experiments (Figure S4) with a 50% inhibitory concentration (IC_{50}) of 5.1 μM. Baicalin and lobeline did not confer dose-dependent suppression of SARS-CoV-2 (Figure S4). We did not pursue the other compound hits because we chose to focus on the only complex extract that yielded antiviral activity at 10 μg/mL with our criteria of <20% cellular toxicity in noninfected cells: the extract of *S. tetrandra*. The three independent preparations of the extract, ST01A, ST01B, and ST01C, showed similar antiviral efficacies of 58.2%, 55.4%, and 57.2% (Figure 1A). Antiviral efficacy was validated in dose−response experiments with each replicate extract of *S. tetrandra* (ST01A, ST01B, and ST01C), yielding IC_{50}s of approximately 1−4 μg/mL, respectively (Figure 1B−D).

Since 36/60 (60%) of the botanical extracts at 10 μg/mL conferred >20% cellular toxicity in Screen 1, we repeated the screen of all the botanical extracts at 1 μg/mL. Plate controls remdesivir at 0.1 μM and camostat at 10 μM conferred 104.7 ± 1.1% and 54.5 ± 1.2% antiviral efficacy, respectively, with no toxicity (Figure S3). No additional extracts with antiviral activity were discovered with this screen, but it did reveal hits with two compounds that were part of the extract plate, verarine and cytisine (Figure S3, Table S1). We did not pursue

https://doi.org/10.1021/acs.jnatprod.3c00159
J. Nat. Prod. 2023, 86, 1061−1073

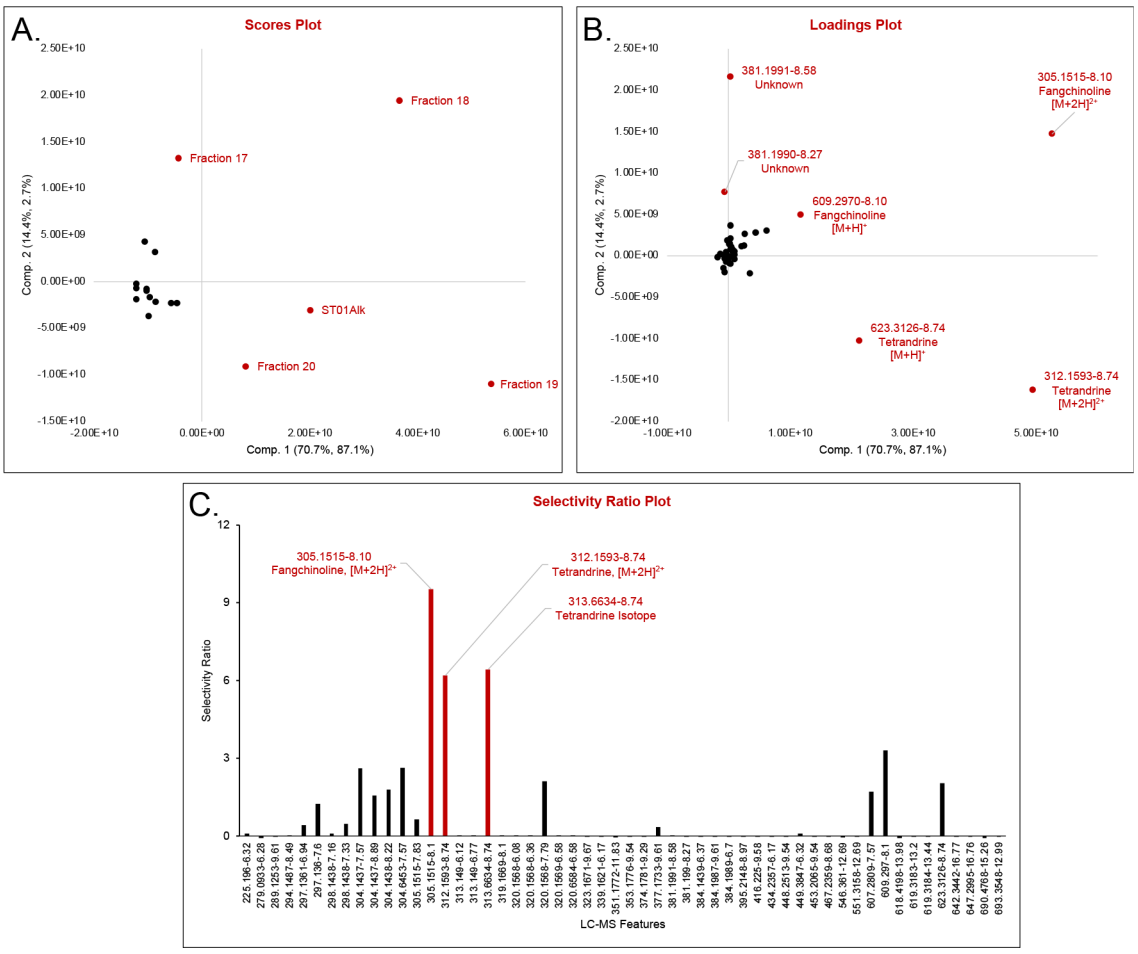

Figure 3. Partial least-squares (PLS) regression analysis predicts *S. tetrandra* alkaloids have antiviral activity. The PLS regression scores plot (A) suggests that F18 and F19 and the alkaloid fraction starting material (ST01ALK) (shown in red) are distinct from the other fractions in their chemical and antiviral activity. Additional fractions for which chemical composition was less strongly correlated with antiviral activity appear near the origin and are shown in black. The PLS loadings plot (B) shows that the $[M + 2H]^{2+}$ features for tetrandrine (**1**) and fangchinoline (**2**) are strongly associated with the antiviral activity of fractions 18 and 19. Two additional features of unknown identity (m/z 381.119, retention times of 8.58 and 8.27) also appear to correlate with activity (B). The selectivity ratio plot (C) predicts antiviral activity for features assigned to fangchinoline (**2**) and tetrandrine (**1**) (shown in red).

these compounds further because we continued to focus on *S. tetrandra*.

To predict constituents from the *S. tetrandra* extracts that were responsible for the antiviral effects, we first partitioned the *S. tetrandra* extract to generate an alkaloid-rich partition (ST01Alk) and separated this partition into fractions using flash chromatography (Figure S5). ST01Alk and its fractions were tested for antiviral efficacy and effects on cell viability on noninfected cells. In parallel, the same samples were profiled using untargeted LC-MS metabolomics. Potent antiviral activity with minimal cytotoxicity was observed for fraction 18 (F18) and fraction 19 (F19; Figure 2, left panel). The LC-MS chromatograms (Figure 2, right panel) of these fractions indicated that, relative to the other fractions, fractions 18 and 19 contained the highest levels of tetrandrine (**1**) and fangchionoline (**2**). Cepharanthine (**3**) and other minor alkaloids of unconfirmed identity were also detected in these fractions. The starting material for the fractionation, ST01Alk, also contained **1**, **2**, and **3** and demonstrated high antiviral activity with minimal cytotoxicity.

To more deeply explore the apparent association between alkaloids and antiviral activity of *S. tetrandra* (Figure 2), partial least-squares (PLS) regression analysis was performed on the LC-MS metabolomics data set using the antiviral data as the dependent variable. As expected, this analysis indicated that F18, F19, and the starting material (ST01Alk) were distinct from the other fractions in the scores plot (Figure 3A). Features associated with the alkaloids fangchinoline (**2**) ($[M + 2H]^{2+}$, m/z 305.1519) and tetrandrine (**1**) ($[M + 2H]^{2+}$, m/z 312.1595) were most strongly associated with antiviral activity, as shown in the loadings plot (Figure 3B). Selectivity ratios were also calculated for the data set. Selectivity ratios serve as a ranking tool for a metabolomics data set;[33] features with high selectivity ratios are more strongly correlated with biological activity (in this case antiviral activity). Compared to the use of PLS scores plots to prioritize active constituents, selectivity ratio analysis has the advantage of being less biased toward highly abundant compounds.[40] Indeed, in agreement with the PLS regression analysis, the selectivity ratio plot generated from this data set (Figure 3C) shows a strong correlation between activity and the features associated with fangchinoline (**2**) and tetrandrine (**1**). Several features in the data set (m/z 381.1991, retention time 8.58, and m/z 381.190, retention time 8.27) were also observed to correlate with antiviral

https://doi.org/10.1021/acs.jnatprod.3c00159
J. Nat. Prod. 2023, 86, 1061−1073

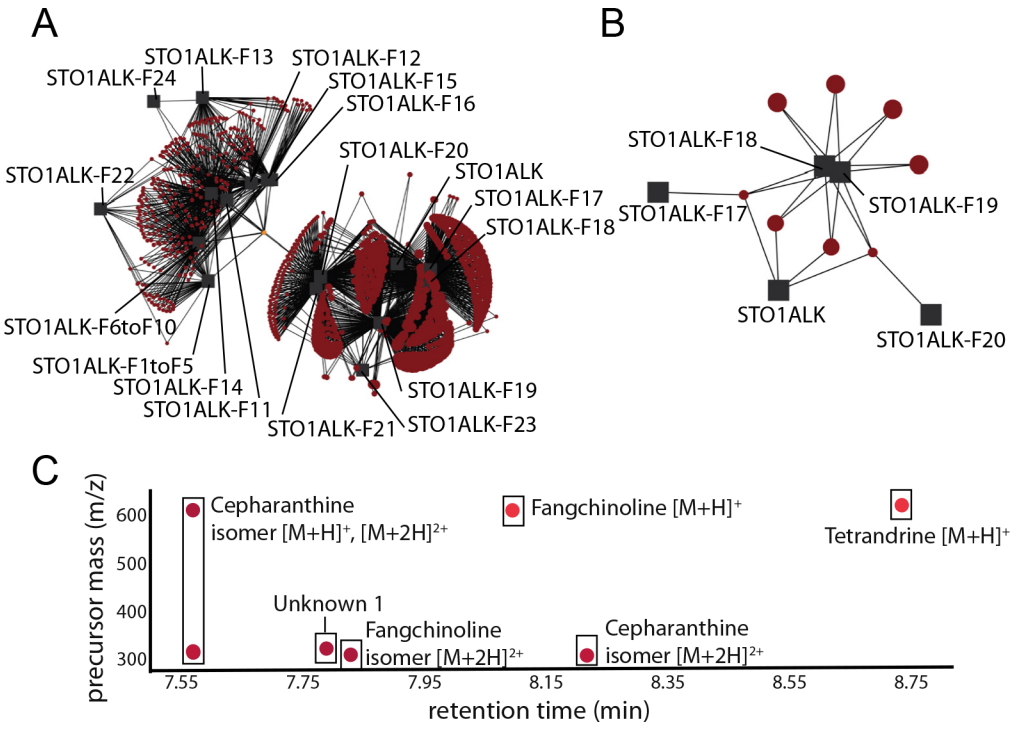

Figure 4. NP Analyst network predicts antiviral activity of *S. tetrandra* alkaloids. (A) NP Analyst network created by using a cluster score of 0.5, activity score of 0, and minimum intensity of 5×10^5. It shows two main clusters of active (large red nodes) and inactive (small red nodes) MS features shared between the extract fractions (gray boxes). (B) NP Analyst network created by using a cluster score of 0.5, activity score of 0.4, and minimum intensity of 5×10^8 showing only the most active and intense MS features (red nodes) and their associated fractions (gray boxes). (C) A scatterplot view of the MS features (precursor mass vs retention time) from panel B and their associated annotations.

efficacy in the selectivity ratio plot (Figure 3C). These compounds were not identified in this study, but based on their similar retention time and mass defect to fangchinoline (**2**) and tetrandrine (**1**) are likely to be additional *S. tetrandra* alkaloids.

As a convergent workflow for assigning active constituents in the *S. tetrandra* extracts and fractions, we employed the newly released NP Analyst[34] platform to integrate the antiviral and metabolomics data sets. NP Analyst is a data integration platform that predicts bioactive constituents from complex mixtures by combining data from screening assays and untargeted metabolomics profiling. The platform works by determining the distribution of mass spectrometry (MS) features across a set of samples and then scoring the strength and consistency of biological profiles for all the samples that a given MS feature is in. MS features are then filtered to retain only those that have both strong activity (activity score) and consistent activity (cluster score) within this set. Finally, these filtered data are presented in several different graphical representations. These include a plot of retention time vs mass-to-charge ratio for all filtered MS features (Figure 4A) and a network graph where square nodes are samples, round nodes are MS features, and edges indicate the presence of a given MS feature in a given sample (Figure 4B). Clustering in this network indicates sets of samples that are related by the presence of one or more shared MS features with predicted biological activity. In agreement with the PLS analysis, NP Analyst showed strong association between antiviral effects and the alkaloid-associated features in the metabolomics data set (Figure 4C).

Collectively, the data in Figures 2−4 predict that alkaloids drive the observed antiviral effects of *S. tetrandra* against SARS-CoV-2 in 293TAT cells. To validate the predictions, we evaluated the purified alkaloids tetrandrine (**1**) and fangchinoline (**2**) for antiviral activity. Since cepharanthine (**3**) has been shown to inhibit other coronaviruses[41] and was also present at low levels in the extract (data not shown), we also tested this alkaloid. Tetrandrine (**1**), fangchinoline (**2**), and cepharanthine (**3**) inhibited SARS-CoV-2 infection with IC_{50}s of 284, 143, and 193 nM, respectively (Figure 5).

To further validate the antiviral potential of *S. tetrandra* alkaloids against SARS-CoV-2, we tested the pure alkaloids for antiviral activity against wild-type virus and the delta variant of concern in Vero E6 cells engineered to overexpress ACE-2 and TMPRSS2, which we abbreviate here as VeroAT cells. The pure alkaloids demonstrated some antiviral activity against the delta variant of concern in VeroAT cells, with cepharanthine (**3**) showing the most potent activity (Figure S6). However, none of the compounds or fractions showed activity against wild-type virus in VeroAT cells (Figure S6). These data suggest that the antiviral activity of *S. tetrandra* extract, fractions, and constituents is variable and likely depends on cellular context.

To gain insight into the cell-type dependency for the antiviral effects, we examined the ability of *S. tetrandra* extracts, fractions, and pure compounds to induce phospholipidosis, which is an accumulation of intracellular phospholipids and is a cellular phenotype that can be induced by small molecules at high μM concentrations.[42] Phospholipidosis has been recently shown to be a potentially confounding effect of antiviral drug repurposing screens.[43] We examined 293TAT and VeroAT cells for phospholipidosis by fluorescence microscopy with a lipid-binding dye upon exposure to *S. tetrandra* alkaloid fractions and pure alkaloids. Sertraline, a cationic amphiphilic

https://doi.org/10.1021/acs.jnatprod.3c00159
J. Nat. Prod. 2023, 86, 1061−1073

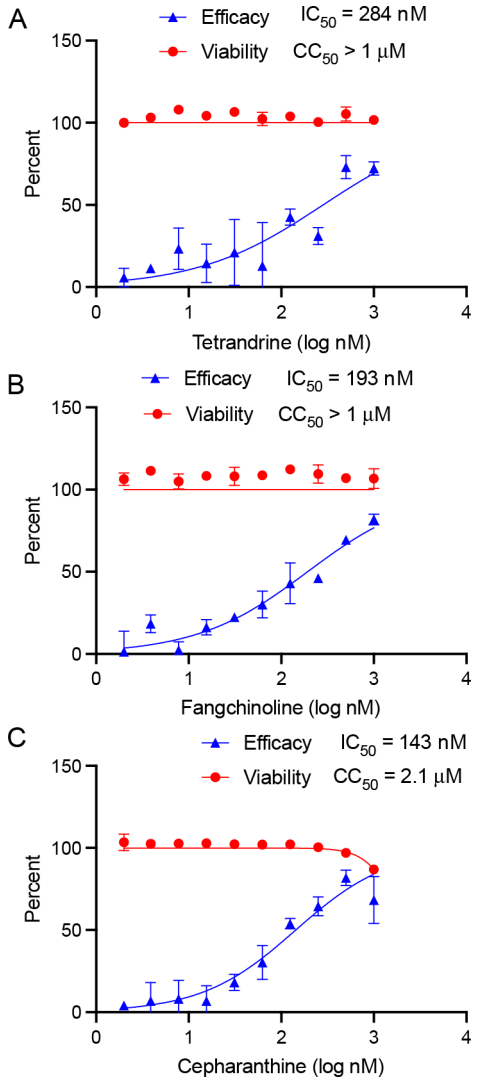

Figure 5. Antiviral effects of *S. tetrandra* alkaloids. 293TAT cells were treated with the indicated concentrations of tetrandrine (**1**) (A), fangchinoline (**2**) (B), or cepharanthine (**3**) (C) prior to infection with SARS-CoV-2 at a multiplicity of infection (MOI) of 0.01. Parallel wells of noninfected cells were treated with the alkaloids to monitor effects on cell viability. After 48 h, cell viability was assessed through measurement of cellular ATP levels. Antiviral effects were quantified in terms of efficacy of the compounds in virus-infected cells, while viability reflects the effects of the extracts on cell health in noninfected cells.

drug (CAD), was used as a positive control at 10 μM for induction of phospholipidosis.[43] Concentrations of 1 μg/mL for extracts and 1 μM for pure alkaloids induced phospholipidosis in 293TAT cells and to a lesser degree in VeroAT cells (Figure S7). However, phospholipidosis was lower when alkaloid concentrations around the 50% inhibitory concentration (IC_{50}) for SARS-CoV-2 (i.e., 100 and 300 nM) were used (Figure S7), suggesting the antiviral effects may be distinct from phospholipidosis. These data further underscore that the cellular responses to *S. tetrandra* vary across cell lines, are suggestive of multiple mechanisms of antiviral action, and emphasize the need for testing in multiple cell lines.

The ability to extrapolate *in vitro* studies to *in vivo* contexts is often limited by concerns that the compounds tested in the *in vitro* assays may not be orally bioavailable. For this study, we took a first step toward addressing this concern by testing *S. tetrandra*, its alkaloid enriched fraction, and purified active components cephranthrine (**3**), fangchinoline (**2**), and tetrandrine (**1**) in the parallel artificial membrane permeability assay (PAMPA). This assay simulates passive diffusion of compounds through a phospholipid bilayer, akin to how compounds are absorbed through the lining of the small intestine and into the bloodstream. The three alkaloids were separately combined into PBS, and their ability to permeate the membrane was compared with a known compound with high diffusivity, verapamil (Figure 6A). While cepharanthine (**3**) and tetrandrine (**1**) displayed comparable diffusivity to the verapamil control in the PAMPA assay, fangchinoline (**2**) demonstrated much less diffusivity (Figure 6A). This may be explained by the additional free hydroxyl in fangchinoline (**2**), which would decrease its ability to diffuse through the trilipid PAMPA membrane.

Interestingly, when the permeabilities of the compounds of interest were compared across conditions (isolated alkaloids, an alkaloid mixture, and *S. tetrandra* extract), additional details emerged suggesting that formulation differentially affects the relative permeability of the active compounds (Figure 6B). Two-way ANOVA revealed significant differences in permeability across compounds and conditions. *Posthoc* tests revealed that both cepharanthine (**3**) and tetrandrine (**1**) were significantly more permeable than fangchinoline (**2**) in all three conditions. Cepharanthine (**3**) as both the isolated alkaloid and as an alkaloid mixture was significantly more permeable than in the *S. tetrandra* extract, while tetrandrine (**1**) was significantly more permeable in the alkaloid mixture as compared to as an isolated alkaloid (Figure 6B). Collectively, the results obtained here with the PAMPA assays suggest that the *S. tetrandra* alkaloids should be biologically available, but that the bioavailability will differ somewhat depending on alkaloid structure and on the other constituents of the matrix (i.e., whether they are administered as isolated compounds, mixtures, or in the context of the extract). Further studies to evaluate metabolism and active transport for these alkaloids and for *S. tetrandra* extracts would also be warranted toward the ultimate goal of extrapolating the *in vitro* results to an *in vivo* context.

To begin to reveal how *S. tetrandra* alkaloid-rich fractions and pure alkaloids modulate 293TAT cell biology during SARS-CoV-2 infection, we performed nCounter gene expression analysis, focusing on the nCounter Immunology panel, which profiles the expression of 594 cellular genes involved in innate immunity and inflammation. We focused on the alkaloid-rich fraction F18 and fangchinoline (**2**) and tetrandrine (**1**) as pure alkaloids since our analysis indicated the majority of the antiviral bioactivity was associated with F18 and these two pure alkaloids (Figure 2). We confirmed the antiviral activity of F18 and the alkaloids, along with the cell-active form molnupiravir (MPV; also known as EIDD-1931, an approved SARS-CoV-2 antiviral drug;[8] Figure S8). Tetrandrine (**1**), fangchinoline (**2**), and F18 conferred robust suppression of SARS-CoV-2 RNAs in virus-infected cells (Figure 7A). Tetrandrine (**1**) and F18 showed more similar patterns of suppression of viral RNAs than fangchinoline (**2**). Moreover, as compared to MPV, tetrandrine (**1**) and F18 showed conferred 2-fold more potent suppression of viral RNAs, such as the viral nucleocapsid N gene, which codes for the nucleocapsid structural protein that protects the viral genome and is involved in packing the RNA into viral particles.

https://doi.org/10.1021/acs.jnatprod.3c00159
J. Nat. Prod. 2023, 86, 1061−1073

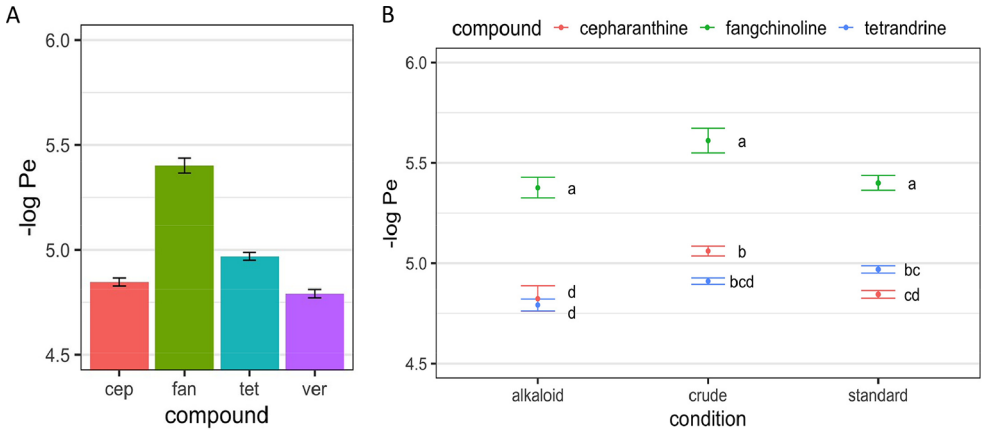

Figure 6. Relative permeabilities of *S. tetrandra* compounds between formulation conditions. PAMPA experiments were performed as described in the Experimental Section. Briefly, samples were loaded into the donor well of the 96-well PAMPA plate. The acceptor plate, filled with the same solvent, was carefully sandwiched on top. The plates were sealed with Teflon tape and left to incubate for 6 h, after which the samples were transferred to mass spectrometry vials for subsequent analysis. (A) Permeability of pure *S. tetrandra* compounds cepharanthine (**3**) (cep), fangchinoline (**2**) (fan), and tetrandrine (**1**) (tet) were incubated along with the high permeability control compound verapamil (ver). High −log Pe values indicate less permeability. Error bars represent SE. (B) Comparison of *S. tetrandra* compounds in different formulations. Standard contains the purified compounds in a combined sample where each was present at 40 μM. Crude extract and alkaloid-enriched fractions were assayed at 400 μg/mL. Error bars represent SE. Letters indicate significant differences among combinations of compounds and conditions as determined by *posthoc* Tukey's HSD pairwise comparisons where $p < 0.05$.

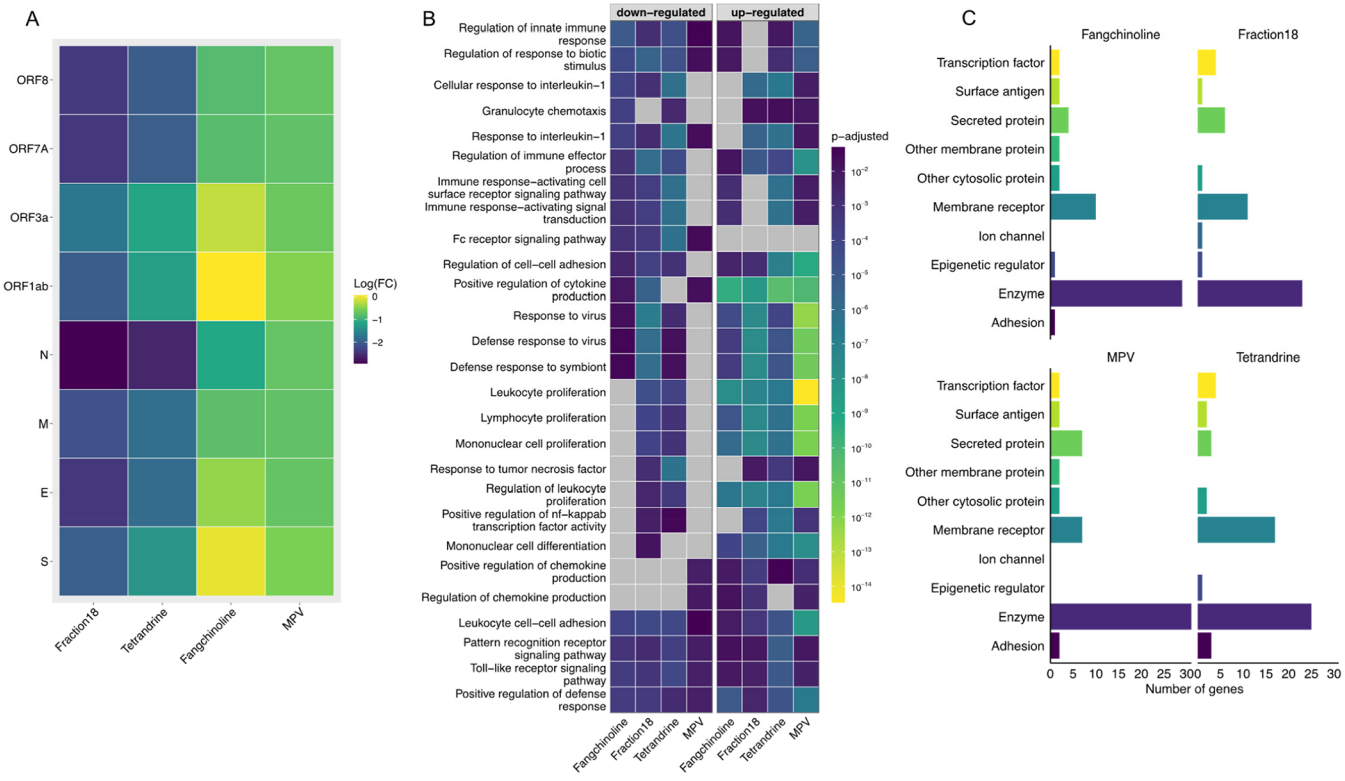

Figure 7. Differential cellular effects of *S. tetrandra* fraction and compounds during SARS-CoV-2 infection in 293TAT cells. Cells were treated for 2 h with fraction 18, fangchinoline (**2**), tetrandrine (**1**), and the cell active form of MPV (EIDD-1931) prior to infection with wild-type SARS-CoV-2. At 24 h postinfection, RNA was extracted from cells (duplicates for each condition), and the expression 594 cellular genes involved in innate immunity and inflammation was measured using the nCounter Immunology panel (Nanostring). (A) Effects of treatments on levels of viral RNAs represented as log2 fold change (FC) relative to infected cells treated with DMSO solvent control. (B) Gene ontology (GO) biological pathway enrichment for top ranked genes based on fold-change upon treatment with compounds relative to infected cells treated with DMSO solvent control. Gray represents no enrichment. (C) Classification of the protein targets for top ranked genes based on fold-change upon treatment with compounds relative to infected cells treated with DMSO solvent control.

Similarly, the ORF1ab gene, which codes for the nonstructural proteins (NSP1−16) that are required for viral transcription, replication, and suppression of host immune response, showed higher suppression by F18 and pure alkaloids compared to MPV. The botanical products suppressed most viral RNA

https://doi.org/10.1021/acs.jnatprod.3c00159
J. Nat. Prod. 2023, 86, 1061−1073

expression to a higher or similar degree to MPV, further confirming their antiviral effects.

Next, we ranked the cellular genes based on their log2 fold-change (logFC > 1 or FC > 2) relative to the DMSO solvent control and shortlisted 100 genes that were perturbed by the selected compounds. Gene enrichment analysis on the ranked genes indicated that F18, tetrandrine (**1**), and fangchinoline (**2**) perturbed cellular genes with similar biological processes that were distinct from MPV (Figure 7B, Supplementary File 2). This was particularly evident in genes that were downregulated by the various treatments. A distinct up-regulation of genes associated with leukocyte proliferation was observed for MPV ($p = 3.57 \times 10^{-15}$), F18, fangchinoline (**2**), and tetrandrine (**1**). Similarly, MPV showed higher up-regulation of cellular genes involved in the host response to virus and related processes as compared to the natural products and F18 (Figure 7B). The results suggest that *S. tetrandra* alkaloids suppress virus infection by multiple mechanisms as compared to MPV's direct suppression of virus replication, which might involve modulation of inflammation through the production of cytokines and other interferon mediators.[44] On the other hand, for down-regulated genes, fangchinoline (**2**) showed no enrichment for many biological processes, which was similar to MPV's lack of down-regulation of many cellular pathways. To further explore the potential mechanisms of action of the *S. tetrandra* fraction and alkaloids, we classified the protein functions of the 100 shortlisted genes and observed that tetrandrine (**1**) modulates many membrane receptors compared to other compounds (Figure 7C). This is in line with the PAMPA studies where tetrandrine (**1**) appeared more permeable than fangchinoline (**2**) (Figure 6). Overall, the transcriptional profiling and pathway analyses suggested that tetrandrine (**1**) and F18 modulate genes in a similar fashion, while fangchinoline (**2**) induced a distinct response in 293TAT cells.

In this report, we deployed multiple chemical, biological, and computational tools to deconvolute the chemical and biological complexity of natural product mixtures. We find that the botanical *S. tetrandra* contains multiple alkaloid compounds that inhibit wild-type SARS-CoV-2 infection in 293TAT cells. The alkaloids and alkaloid fraction also inhibited the delta variant of concern but not wild-type SARS-CoV-2 in Vero cells expressing TMPRSS2 and ACE-2. The alkaloids also possess potential drug-like activity based on their ability to penetrate artificial membranes. A focused transcriptional study showed that *S. tetrandra* alkaloids can only partially reverse virus-induced changes in cellular gene expression, indicating that the mechanism(s) by which this botanical and its constituents inhibits *in vitro* SARS-CoV-2 infection requires further study.

Our studies demonstrating the antiviral potential of *S. tetrandra* alkaloids in certain cellular contexts align with previous studies. For example, tetrandrine (**1**) has been reported to inhibit Ebola virus[45,46] and SARS-CoV-2[47,48] infection of VeroAT cells. In addition to tetrandrine (**1**), other alkaloids in *S. tetrandra* including fangchinoline (**2**) and cepharanthine (**3**) have also been shown to inhibit human coronavirus HCoV-OC43 infection of MRC5 human lung cells[41] and MERS-CoV.[49] However, we found that the antiviral activity was not uniform across cell lines, and some of this activity may be associated with induction of phospholipidosis, especially at high concentrations of fractions or pure compounds. Since phospholipidosis has recently been reported to be a potential artifact in drug-based antiviral screens,[43] the antiviral potential of *S. tetrandra* and likely many other botanical compounds should be approached with careful and rigorous scrutiny. Moreover, much of the literature on *in vitro* effects of tetrandrine (**1**) appear to occur at relatively high micromolar concentrations.[50] Considering that phospholipidosis rarely occurs at concentrations below 100 nM[43] and that the pure alkaloids had IC_{50} concentrations in this range (Figure 2), it might be possible to improve the selectivity and potency of these compounds either by designing more potent analogs or testing compounds in combination, which we have shown confers superior antiviral potency through synergism.[23,51,52] Moreover, the differences in the permeability of the alkaloids in various mixtures (Figure 6) could likely inform future studies aimed at enhancing the antiviral potency of these compounds. Mechanistic studies are required to discern whether alkaloids inhibit virus infection by directly blocking viral enzymes or proteins versus cellular targets. In terms of cellular targeting as a mechanism to inhibit virus infection tetrandrine (**1**), fangchinoline (**2**) and cepharanthine (**3**) have been shown or proposed to block many cellular pathways to confer antiviral effects,[45,50] and some studies show that these alkaloids block virus entry and intracellular trafficking.[45,49,53] In this regard, our cell culture infectivity model incorporates TMPRSS2-primed, Spike protein-mediated virus entry via fusion at the cell membrane.[37]

In closing, we describe comprehensive chemical, biological, and computational approaches to connect natural product chemical complexity with antiviral activity in the context of *in vitro* SARS-CoV-2 infection. Our results emphasize the need for rigorous approaches to this endeavor. While botanicals like *S. tetrandra* confer antiviral effects against SARS-CoV-2 *in vitro*, this activity is dependent on cell type. Thus, cell context specificity is a critical factor when identifying natural product modulators of viral infection. As such, this study should not be considered an endorsement of the use of *S. tetrandra* for the treatment of SARS-CoV-2 infection. Preclinical and clinical studies are necessary to establish safety and efficacy. Notably, several previous studies of the pure alkaloid tetrandrine (**1**) and an *S. tetrandra* extract have demonstrated toxicity in mouse and rat models.[29] Thus, toxicity could be a concern in a clinical context.

EXPERIMENTAL SECTION

Natural Products and Botanical Extracts. The library consisted of 173 pure compounds purchased from Chromadex and 60 separate extracts prepared from six different botanical species. Details of the pure compounds and complex botanical extracts including compound classes, names, sources of extracts, and Certificates of Authenticity can be found in Figures S1, S2, and S11.

Cell Culture and Live Virus. 293TAT cells were generated as described[37] and maintained in Dulbecco's modified Eagle medium (DMEM; Gibco, 11995) supplemented with 9% fetal bovine serum (FBS; HyClone SH3007103) and 1% penicillin−streptomycin (Gibco, 15140), 1× nonessential amino acids (NEAA; Gibco 11140), and 20 mM HEPES (Gibco 15630). Vero E6 African Green Monkey kidney epithelial cells expressing transmembrane protease, serine 2, and human angiotensin-converting enzyme 2 (Vero E6-TMPRSS2-T2A-ACE2; referred to here as VeroAT cells) were obtained from BEI Resources (NR-54970) and provided by Tien-Ying Hsiang and Michael Gale. These cells were maintained in DMEM supplemented with 5% FBS, 1% penicillin−streptomycin, and 10 μg/mL puromycin.

Wild-type, infectious SARS-CoV-2 (BEI Resources; Isolate USA-WA1/2020 NR-52281) and the SARS-CoV-2 variant of concern stock

https://doi.org/10.1021/acs.jnatprod.3c00159
J. Nat. Prod. 2023, 86, 1061−1073

of delta virus were obtained from Tien-Ying Hsiang and Michael Gale and were generated as described.[52]

Drug Treatment and Infection of Cells with Live Virus. Compounds, extracts, or fractions were added to cells, followed immediately by addition of live virus (SARS-CoV-2 WA1 or the delta variant of concern) stock to each infected well or virus-free medium to each uninfected well. Plates were incubated at 37 °C, 5% CO_2 for 48 h for live virus experiments.

Cell Viability Assay. For drug dose−response studies, we measured cell viability in parallel wells using the CellTiter-Glo 2.0 assay (Promega, G9243). The assay measures the presence of metabolically active cells by quantifying cellular ATP levels. The contents of each well were aspirated, followed by the addition of 50 μL of phosphate-buffered saline (PBS; Gibco, 10010031) and 50 μL of CellTiter-Glo reagent. The plate was then shaken for 2 min, incubated at room temperature for 10 min, then read for luminescence on a Biotek Synergy H4 plate reader.

LC-MS Data Acquisition for Collection of Metabolomics Data. LC-MS data were acquired using a Q Exactive Plus quadrupole-Orbitrap mass spectrometer (ThermoFisher Scientific) with a heated electrospray ionization (HESI) source coupled with an Acquity UPLC system (Waters, Milford, MA, USA). Samples were suspended in methanol at a concentration of 100 μg/mL. Randomized triplicate injections of 5 μL were eluted from an Acquity UPLC BEH C_{18} column (1.7 μM, 2.1 × 50 mm, Waters) at a flow rate of 0.3 mL/min. A binary solvent gradient of water with 0.1% ammonium hydroxide (A) and acetonitrile with 0.1% ammonium hydroxide (B) was used. The gradient began at 2% B, followed by a linear increase to 20%, 30%, 55%, 80%, and then 90% B over 23.0 min. An isocratic hold was performed at 90% B for 2 min before returning to starting conditions to allow equilibration for 6.0 min prior to the next injection. The mass spectrometer was operated in the positive ionization mode over a full scan of m/z 120−1800 with the following instrument parameters: capillary temperature, 256 °C; spray voltage, 3.00 kV; sheath gas, 48 arbitrary units; auxiliary gas, 11 arbitrary units; spare gas, 2 arbitrary units; and probe heater temperature, 350 °C.

To confirm identities of alkaloids, standards of tetrandrine (Cayman Chemical Company Item No. 19874, ≥98% purity), cepharanthine (Cayman Chemical Company Item No. 19648, ≥98% purity), and fangchinoline (Cayman Chemical Company Item No. 29243, ≥98% purity) were prepared at a final concentration of 0.625 μM in methanol. The standards were analyzed in parallel with the extracts, and fragmentation spectra were acquired with data-dependent MS-MS using a collision energy of 30 V. Fragmentation patterns, retention times, and accurate mass were compared for the reference standards and putative alkaloids in the extracts and fractions.

Metabolomics Data Analysis. LC-MS raw files were centroided using MSConvert ProteoWizard 3.0,[54] then imported to MZmine 2.53[55] for peak picking to create a list of MS features (m/z-RT). Methods include mass detection, chromatogram building, chromatogram deconvolution, deisotoping, feature alignment, gap filling, duplicate filtering, and peak filtering. The parameters used are in Figure S9. The final feature lists were imported to MS Excel for further treatment.

The feature list was filtered for background noise, which may be due to contaminants in the solvent of the LC-MS system. The first step included removing features with a relative standard deviation (RSD) lower than 30% across all samples. This step removes ubiquitous high-quality features such as background noise. The next step was to remove features that were more abundant in the blanks than in the samples. This was done by taking the percent ratio of the average peak area of the feature across all the solvent blanks and the average peak area of the feature across all of the samples. All features with a percent ratio of more than 80% were deleted from the feature list. The final step was to remove poor-quality features in the samples based on the RSD of the peak area of every sample in triplicate. Features in specific samples with a peak area RSD greater than 35% were removed from that sample. Mass spectral features that did not vary in intensity across samples based on a cutoff of ≤0.02% of the highest variance were removed from the data set.

Partial Least-Squares Regression Analysis and Calculation of Selectivity Ratios. The preprocessed data set was imported to Sirius 11.5 (Pattern Recognition Systems AS, Bergen, Norway) for statistical analysis, using the features in the peak list as the independent variables and the antiviral efficacy of each sample as the dependent variable. The data were analyzed using partial-least-squares regression followed by calculation of selectivity ratios (SR), which is the ratio of the explained variance of the data set and the unexplained variance. The SR reveals features that have high correlation with a measured biological activity and thus can be used to predict potential biologically active compounds from a complex mixture.[56−59] The data set was validated leaving out one object with 100 repetitions and a significance level of 0.5 to determine the number of PLS regression components to be used in the modeling.

NP Analyst. A .csv file containing the antiviral and cell viability data normalized between 0 and 1 was uploaded to NP Analyst (www.npanalyst.org) along with an MZmine 2.53[55] export table containing the m/z, retention times, and peak areas for mass features from all samples. Data were analyzed using two different sets of settings: activity score: 0, cluster score: 0.5, MS intensity threshold: 5×10^5 to profile all MS features associated with bioactive extracts, and activity score: 0.4, cluster score 0.5, MS intensity threshold: 1×10^7 to interrogate MS features with the strongest predicted bioactivity profiles.

Fluorescence Microscopy for Phospholipidosis. Cells were treated with pure alkaloids or alkaloid-rich fractions in the presence of 1× HCS LipidTOX dye (Thermo Fisher H34350). Sertraline (SERT) at 10 μM was added to cells as a positive control for induction of phospholipidosis. At 24 h postinfection, medium was removed from cell cultures, and cells were washed in PBS and fixed in 4% paraformaldehyde for 20 min at room temperature. Cells were then washed twice in PBS and then stained with DAPI and imaged using Cytation 1 cell imaging system (BioTek, Winooski, VT, USA) using a 10× objective and light cubes for DAPI (nuclear stain) and GFP (LipidTOX dye). Gen5 software (Biotek) was used for image acquisition, processing, and subsequent analysis. The 10× objective was used to take 64 individual images using an 8 × 8 matrix, which were stitched together utilizing Gen5's montage feature. The DAPI threshold was set at 5000 relative fluorescent units, and the GFP threshold was set at 15,000 relative fluorescent units to identify nuclei and GFP surrounding cells, respectively. Analysis identifying nuclei in the DAPI channel utilized a minimum and maximum size selection of 5 to 100 μm and 2 to 200 μm to capture stained nuclei of VeroAT and 293TAT cells, respectively. GFP-positive cells were identified utilizing minimum and maximum size selection as in the DAPI channel with a 5 μm expansion from primary DAPI mask to capture only GFP surrounding cells.

PAMPA Assay and Permeability Analyses. PAMPA experiments were run using a Corning BioCoat pre-coated PAMPA plate system according to the manufacturer's protocol. Control compounds including methotrexate (low-permeability control), verapamil (high-permeability control), and sulfasalazine (low-permeability, colored PAMPA membrane integrity indicator) as well as pure *S. tetrandra* metabolite standards, cepharanthrine, fangchinoline, and tetrandrine, were dissolved in DMSO to a stock concentration of 1 mM and diluted with PBS (pH 7.4) to a final concentration of 40 μM containing 4% DMSO. Crude extracts and alkaloid-enriched fractions were dissolved in DMSO to a stock concentration of 10 mg/mL. Stock solutions were then dissolved in PBS (pH 7.4) to a final concentration of 400 μg/mL containing 4% DMSO. A 300 μL portion of each sample (n = 6 replicates per condition) were added to donor plate wells. A 200 μL amount of 4% DMSO in PBS (pH 7.4) was also added to each of the acceptor plate wells, and the two were joined and sealed with parafilm to prevent evaporation and incubated at room temperature for 5 h. At the end of the incubation period, 100 mL aliquots were removed from the donor and acceptor wells and transferred to mass spectrometry vials with low-volume inserts for subsequent LC-MS analysis. Samples were stored at −80 °C prior to further analysis and vortexed upon thawing.

https://doi.org/10.1021/acs.jnatprod.3c00159
J. Nat. Prod. 2023, 86, 1061−1073

LC-MS data were acquired using an Acquity I-Class UPLC system coupled to a Waters G2-XS ESI-QToF mass spectrometer (Waters, Milford, MA, USA). Samples were chromatographed on an Acquity UPLC BEH C18 1.8 μm, 2.1 × 100 mm column (Waters) with a flow rate of 0.40 mL/min and a binary solvent gradient consisting of H_2O with 0.1% ammonium hydroxide (solvent A) and ACN (solvent B). The solvent gradient was as follows: initial isocratic hold at 98% A for 0.5 min then increasing linearly to 20% B at 2.5 min followed by an increase to 80% B at 10.5 min and to 98% B at 11.5 min. This was followed by an isocratic hold for 2 min, a return to initial conditions over 0.1 min, and re-equilibration for 2 min prior to the next injection. Mass spectral data were acquired with simultaneous acquisition of a lockmass solution (leucine encephalin) in continuum mode with the MS^E function (mass range 50−1800 Da; scan time 0.1 scans/s; function 1 CE off; function 2 CE ramp 35−45 V over a scan range of m/z 50−1800 Da. Spectrometer settings were as follows: source temperature ∼100 °C, desolvation temperature ∼550 °C, cone gas flow ∼100 L/h, and desolvation gas flow ∼800 L/h. Relative concentrations used in permeability calculations were determined using peak areas from EIC chromatograms for each compound in the donor and acceptor wells. Donor and acceptor wells were diluted 10× prior to LC-MS analysis to obtain appropriate peak shape and intensity. Permeability was determined using the integrated EIC peak areas of the compounds in the donor and acceptor wells at the end of the PAMPA assay and the calculations shown in Figure S10.[60]

A two-way analysis of variance (ANOVA) was used to compare permeability across compounds (cepharanthine, fangchinoline, tetrandrine) and conditions (alkaloid, crude, standard). Permeability values were cube-root transformed in order to meet assumptions of normality and homoscedasticity. When significant differences were detected ($\alpha < 0.05$), a *posthoc* Tukey test was conducted to test for pairwise differences among combinations of conditions and compounds. Statistical analyses were performed in R (v4.1.0; R Core Team 2016; https://www.r-project.org/).

Antiviral Assay Data Analyses. For single-drug experiments, drug concentrations were log transformed, and the concentration of drug(s) that inhibited virus by 50% (i.e., IC_{50}) and the concentration of drug(s) that killed 50% of cells (i.e., CC_{50}) were determined via nonlinear logistic regressions of log(inhibitor) versus response-variable dose−response functions (four parameters) constrained to zero bottom asymptote by statistical analysis using GraphPad Prism 9 (GraphPad Software, Inc.) as described.[51]

Gene Expression Analyses. 293TAT cells were infected or not infected with wild-type SARS-COV-2, and virus-infected cells were also treated with molnupiravir, tetrandrine, fangchinoline, and fraction 18 of the alkaloid-rich fraction ST01ALK-F18. Cells were treated with compounds and infected under BSL3 containment as described above. Cells were lysed in DNA/RNA Shield (Zymo Research ZR120025), RNA was extracted with Monarch total RNA miniprep kit (NEB T2010S), and yield was determined using a Nanodrop ND-100 spectrophotometer (ThermoFisher). RNA integrity was determined using Agilent Tape station 4150 (Agilent Technologies, Seattle, WA, USA). mRNA transcript abundance was measured from 150 ng of RNA using the nCounter host immune response (LBL-10805-01). The host response panel consisted of 773 genes and 12 housekeeping genes. Briefly, 70 μL of hybridization buffer was added to Reporter CodeSet to prepare the master mix. To set up the hybridization reactions, each sample tube contained 8 μL of master mix and 5 μL of diluted RNA sample. Capture ProbeSet (2 μL) was added to each tube, and samples were hybridized at 65 °C for 18 h. Quality control of nCounter data, data normalization, and gene expression differences were performed using nSolver and Advanced Analysis version 2.0.

Bioinformatics Analyses. We used the normalized Nanostring gene expression data for further downstream bioinformatics analysis. The fold-change was computed using the limma package in R.[61] The log2 fold-change was computed for infected cells treated with natural products (fraction 18, fangchinoline, tetrandrine) and MPV versus virus-infected cells treated with DMSO solvent control. The genes with a log2 fold-change greater than 1 were selected and then converted into fold-change (Supplementary File 1). Since we only had two replicates for each condition, we performed all analysis on the fold-change rather than differential expression analysis, since the statistical tests would perform poorly with such limited number of replicates. Codes for data analysis can be found at GitHub: https://github.com/RavindranVandana/Modulation_SARS-CoV-2_botanical_extract_S_tetrandra

To further shortlist the genes, we ranked the genes with highest fold-change and selected the top 100 ranked genes for further gene enrichment analysis. Based on the value of the log2 fold-change we marked the genes as up- and down-regulation. For each gene its UniProt ID was retrieved using the UniProt mapping tool.[62] The protein class for each gene was retrieved from ChEMBL.[63] Gene enrichment and ontology (GO) analysis was performed using the ClusterProfiler package in R[64,65] (Supplementary File 2).

■ ASSOCIATED CONTENT

Supporting Information

The Supporting Information is available free of charge at https://pubs.acs.org/doi/10.1021/acs.jnatprod.3c00159.

Figures S1−S11: Supporting figures (PDF)

Supplementary File 1: Gene expression (XLSX)

Supplementary File 2: GO analysis (XLSX)

Table S1: All raw screening data (XLSX)

■ AUTHOR INFORMATION

Corresponding Author

Stephen J. Polyak − *Department of Laboratory Medicine and Pathology, University of Washington, Seattle, Washington 98195, United States;* orcid.org/0000-0001-7475-9827; Phone: 206-861-5764; Email: polyak@uw.edu

Authors

Aswad Khadilkar − *Department of Chemistry and Biochemistry, University of California, Santa Cruz, California 95964, United States*

Zoie L. Bunch − *Department of Chemistry and Biochemistry, University of North Carolina, Greensboro, North Carolina 27412, United States*

Jessica Wagoner − *Department of Laboratory Medicine and Pathology, University of Washington, Seattle, Washington 98195, United States*

Vandana Ravindran − *Oslo Centre for Biostatistics and Epidemiology (OCBE), Faculty of Medicine, University of Oslo, Oslo 0313, Norway*

Jessica M. Oda − *Department of Laboratory Medicine and Pathology, University of Washington, Seattle, Washington 98195, United States*

Warren S. Vidar − *Department of Chemistry and Biochemistry, University of North Carolina, Greensboro, North Carolina 27412, United States*

Trevor N. Clark − *Department of Chemistry, Simon Fraser University, Burnaby, BC V5A 1S6, Canada*

Preston K. Manwill − *Department of Chemistry and Biochemistry, University of North Carolina, Greensboro, North Carolina 27412, United States;* orcid.org/0000-0002-6072-1067

Daniel A. Todd − *Department of Chemistry and Biochemistry, University of North Carolina, Greensboro, North Carolina 27412, United States*

Sarah A. Barr − *Department of Chemistry and Biochemistry, University of North Carolina Wilmington, Wilmington, North Carolina 28403, United States*

Lauren K. Olinger − *Department of Biology and Marine Biology, University of North Carolina Wilmington, Wilmington, North Carolina 28403, United States*
Susan L. Fink − *Department of Laboratory Medicine and Pathology, University of Washington, Seattle, Washington 98195, United States;* orcid.org/0000-0003-1705-0103
Wendy K. Strangman − *Department of Chemistry and Biochemistry, University of North Carolina Wilmington, Wilmington, North Carolina 28403, United States;* orcid.org/0000-0002-6911-4909
Roger G. Linington − *Department of Chemistry, Simon Fraser University, Burnaby, BC V5A 1S6, Canada;* orcid.org/0000-0003-1818-4971
John B. MacMillan − *Department of Chemistry and Biochemistry, University of California, Santa Cruz, California 95964, United States;* orcid.org/0000-0003-1430-1077
Nadja B. Cech − *Department of Chemistry and Biochemistry, University of North Carolina, Greensboro, North Carolina 27412, United States;* orcid.org/0000-0001-6773-746X

Complete contact information is available at: https://pubs.acs.org/10.1021/acs.jnatprod.3c00159

Author Contributions

The manuscript was written through contributions of all authors. All authors have given approval to the final version of the manuscript.

Funding

This work was supported by supported by the National Center for Complementary and Integrative Health (NCCIH) and the Office of Dietary Supplements (ODS), components of the National Institutes of Health, under grant numbers 3U41AT008718-07S1 (to J.M. and S.J.P.) and 5U41AT008718-08 (to J.M., N.C., and R.L.). Z.L.B. received support from T32AT008938 from the NCCIH. S.L.F. received support from R01AI162684 (NIAID). S.J.P. received support from the Department of Laboratory Medicine and Pathology (University of Washington). V.R. was supported from the European Union's Horizon 2020 Research and Innovation program under the Marie Skłodowska-Curie Actions Grant, agreement No. 80113 (Scientia fellowship).

Notes

The authors declare no competing financial interest.

■ ACKNOWLEDGMENTS

The following reagents were deposited by the Centers for Disease Control and Prevention and obtained through BEI Resources, NIAID, NIH: SARS-Related Coronavirus 2, Isolate USA-WA1/2020, NR-52281. *Cercopithecus aethiops* kidney epithelial cells expressing transmembrane protease, serine 2 and human angiotensin-converting enzyme 2 (Vero E6-TMPRSS2-T2A-ACE2, NR-54970, referred to in this paper as VeroAT cells) were also obtained from BEI Resources. We thank Michael Gale, Jr., and Tien-Ying Hsiang for providing the delta VOC stock and VeroAT cells, Carol Weiss for providing the 293TAT cell line, and Judith White for insightful discussions.

■ REFERENCES

(1) Bixler, S. L.; Bocan, T. M.; Wells, J.; Wetzel, K. S.; Van Tongeren, S. A.; Dong, L.; Garza, N. L.; Donnelly, G.; Cazares, L. H.; Nuss, J.; Soloveva, V.; Koistinen, K. A.; Welch, L.; Epstein, C.; Liang, L.-F.; Giesing, D.; Lenk, R.; Bavari, S.; Warren, T. K. *Antiviral-research* **2018**, *151*, 97−104.
(2) Group, P. I. W.; Multi-National, P. I. I. S. T.; Davey, R. T., Jr; Dodd, L.; Proschan, M. A.; Neaton, J.; Neuhaus Nordwall, J.; Koopmeiners, J. S.; Beigel, J.; Tierney, J.; Lane, H. C.; Fauci, A. S.; Massaquoi, M. B. F.; Sahr, F.; Malvy, D. *New-England-Journal-of-Medicine.* **2016**, *375* (15), 1448−1456.
(3) Maxmen, A. *Nature* **2019**, *572* (7767), 16−17.
(4) Mulangu, S.; Dodd, L. E.; Davey, R. T., Jr; Tshiani Mbaya, O.; Proschan, M.; Mukadi, D.; Lusakibanza Manzo, M.; Nzolo, D.; Tshomba Oloma, A.; Ibanda, A.; Ali, R.; Coulibaly, S.; Levine, A. C.; Grais, R.; Diaz, J.; Lane, H. C.; Muyembe-Tamfum, J. J.; Group, P. W.; Sivahera, B.; Camara, M.; Kojan, R.; Walker, R.; Dighero-Kemp, B.; Cao, H.; Mukumbayi, P.; Mbala-Kingebeni, P.; Ahuka, S.; Albert, S.; Bonnett, T.; Crozier, I.; Duvenhage, M.; Proffitt, C.; Teitelbaum, M.; Moench, T.; Aboulhab, J.; Barrett, K.; Cahill, K.; Cone, K.; Eckes, R.; Hensley, L.; Herpin, B.; Higgs, E.; Ledgerwood, J.; Pierson, J.; Smolskis, M.; Sow, Y.; Tierney, J.; Sivapalasingam, S.; Holman, W.; Gettinger, N.; Vallee, D.; Nordwall, J.; Team, P. C. S. *New-england-journal-of-medicine.* **2019**, *381* (24), 2293−2303.
(5) Beigel, J. H.; Tomashek, K. M.; Dodd, L. E.; Mehta, A. K.; Zingman, B. S.; Kalil, A. C.; Hohmann, E.; Chu, H. Y.; Luetkemeyer, A.; Kline, S.; Lopez de Castilla, D.; Finberg, R. W.; Dierberg, K.; Tapson, V.; Hsieh, L.; Patterson, T. F.; Paredes, R.; Sweeney, D. A.; Short, W. R.; Touloumi, G.; Lye, D. C.; Ohmagari, N.; Oh, M. D.; Ruiz-Palacios, G. M.; Benfield, T.; Fatkenheuer, G.; Kortepeter, M. G.; Atmar, R. L.; Creech, C. B.; Lundgren, J.; Babiker, A. G.; Pett, S.; Neaton, J. D.; Burgess, T. H.; Bonnett, T.; Green, M.; Makowski, M.; Osinusi, A.; Nayak, S.; Lane, H. C.; Members, A.-S. G. *New-England-Journal-of-Medicine* **2020**, *383*, 1813.
(6) Spinner, C. D.; Gottlieb, R. L.; Criner, G. J.; Arribas Lopez, J. R.; Cattelan, A. M.; Soriano Viladomiu, A.; Ogbuagu, O.; Malhotra, P.; Mullane, K. M.; Castagna, A.; Chai, L. Y. A.; Roestenberg, M.; Tsang, O. T. Y.; Bernasconi, E.; Le Turnier, P.; Chang, S. C.; SenGupta, D.; Hyland, R. H.; Osinusi, A. O.; Cao, H.; Blair, C.; Wang, H.; Gaggar, A.; Brainard, D. M.; McPhail, M. J.; Bhagani, S.; Ahn, M. Y.; Sanyal, A. J.; Huhn, G.; Marty, F. M.; Investigators, G.-U.-. *JAMA* **2020**, *324* (11), 1048−1057.
(7) Sheahan, T. P.; Sims, A. C.; Zhou, S.; Graham, R. L.; Pruijssers, A. J.; Agostini, M. L.; Leist, S. R.; Schafer, A.; Dinnon, K. H., 3rd; Stevens, L. J.; Chappell, J. D.; Lu, X.; Hughes, T. M.; George, A. S.; Hill, C. S.; Montgomery, S. A.; Brown, A. J.; Bluemling, G. R.; Natchus, M. G.; Saindane, M.; Kolykhalov, A. A.; Painter, G.; Harcourt, J.; Tamin, A.; Thornburg, N. J.; Swanstrom, R.; Denison, M. R.; Baric, R. S. An orally bioavailable broad-spectrum antiviral inhibits SARS-CoV-2 in human airway epithelial cell cultures and multiple coronaviruses in mice. *Sci. Transl. Med.* **2020**, *12* (541), DOI: 10.1126/scitranslmed.abb5883.
(8) Mahase, E. *BMJ.* **2021**, *375*, n2422.
(9) Couzin-Frankel, J. *Science* **2021**, *374* (6569), 799−800.
(10) Fischer, W. A., 2nd; Eron, J. J., Jr; Holman, W.; Cohen, M. S.; Fang, L.; Szewczyk, L. J.; Sheahan, T. P.; Baric, R.; Mollan, K. R.; Wolfe, C. R.; Duke, E. R.; Azizad, M. M.; Borroto-Esoda, K.; Wohl, D. A.; Coombs, R. W.; James Loftis, A.; Alabanza, P.; Lipansky, F.; Painter, W. P. *Sci. Transl Med.* **2022**, *14* (628), No. eabl7430.
(11) Hammond, J.; Leister-Tebbe, H.; Gardner, A.; Abreu, P.; Bao, W.; Wisemandle, W.; Baniecki, M.; Hendrick, V. M.; Damle, B.; Simon-Campos, A.; Pypstra, R.; Rusnak, J. M.; Investigators, E.-H. *New-england-journal-of-medicine.* **2022**, *386* (15), 1397−1408.
(12) Mahase, E. *BMJ.* **2021**, *375*, n2713.
(13) Jochmans, D.; Liu, C.; Donckers, K.; Stoycheva, A.; Boland, S.; Stevens, S. K.; De Vita, C.; Vanmechelen, B.; Maes, P.; Trüeb, B.; Ebert, N.; Thiel, V.; De Jonghe, S.; Vangeel, L.; Bardiot, D.; Jekle, A.; Blatt, L. M.; Beigelman, L.; Symons, J. A.; Raboisson, P.; Chaltin, P.; Marchand, A.; Neyts, J.; Deval, J.; Vandyck, K. *bioRxiv* **2022**, 2022.06.07.495116.
(14) Zhou, Y.; Gammeltoft, K. A.; Ryberg, L. A.; Pham, L. V.; Fahnøe, U.; Binderup, A.; Hernandez, C. R. D.; Offersgaard, A.;

Fernandez-Antunez, C.; Peters, G. H. J.; Ramirez, S.; Bukh, J.; Gottwein, J. M. *bioRxiv* **2022**, 2022.06.06.494921.
(15) Flynn, J. M.; Samant, N.; Schneider-Nachum, G.; Barkan, D. T.; Yilmaz, N. K.; Schiffer, C. A.; Moquin, S. A.; Dovala, D.; Bolon, D. N. A. *Elife* **2022**, *11*, No. e77433.
(16) Heilmann, E.; Costacurta, F.; Volland, A.; von Laer, D. *bioRxiv* **2022**, 2022.07.02.495455.
(17) Iketani, S.; Mohri, H.; Culbertson, B.; Hong, S. J.; Duan, Y.; Luck, M. I.; Annavajhala, M. K.; Guo, Y.; Sheng, Z.; Uhlemann, A.-C.; Goff, S. P.; Sabo, Y.; Yang, H.; Chavez, A.; Ho, D. D. *bioRxiv* **2022**, 2022.08.07.499047.
(18) Szemiel, A. M.; Merits, A.; Orton, R. J.; MacLean, O. A.; Pinto, R. M.; Wickenhagen, A.; Lieber, G.; Turnbull, M. L.; Wang, S.; Furnon, W.; Suarez, N. M.; Mair, D.; da Silva Filipe, A.; Willett, B. J.; Wilson, S. J.; Patel, A. H.; Thomson, E. C.; Palmarini, M.; Kohl, A.; Stewart, M. E. *PLoS Pathog* **2021**, *17* (9), No. e1009929.
(19) Checkmahomed, L.; Carbonneau, J.; Du Pont, V.; Riola, N. C.; Perry, J. K.; Li, J.; Pare, B.; Simpson, S. M.; Smith, M. A.; Porter, D. P.; Boivin, G. *Antimicrob. Agents Chemother.* **2022**, *66* (7), No. e0019822.
(20) Hogan, J. I.; Duerr; Dimartino, D.; Marier, C.; Hochman, S.; Mehta, S.; Wang, G.; Heguy, A., Remdesivir resistance in transplant recipients with persistent COVID-19. *Res. Sq* **2022**.
(21) Moghadasi, S. A.; Heilmann, E.; Moraes, S. N.; Kearns, F. L.; von Laer, D.; Amaro, R. E.; Harris, R. S., Transmissible SARS-CoV-2 variants with resistance to clinical protease inhibitors. *bioRxiv* **2022**.
(22) Hu, Y.; Lewandowski, E. M.; Tan, H.; Morgan, R. T.; Zhang, X.; Jacobs, L. M. C.; Butler, S. G.; Mongora, M. V.; Choy, J.; Chen, Y.; Wang, J. *bioRxiv* **2022**, 2022.06.28.497978.
(23) White, J. M.; Schiffer, J. T.; Bender Ignacio, R. A.; Xu, S.; Kainov, D.; Ianevski, A.; Aittokallio, T.; Frieman, M.; Olinger, G. G.; Polyak, S. J. *mBio* **2021**, *12* (6), No. e0334721.
(24) Hamulka, J.; Jeruszka-Bielak, M.; Gornicka, M.; Drywien, M. E.; Zielinska-Pukos, M. A. *Nutrients* **2021**, *13* (1), 54.
(25) Lam, C. S.; Koon, H. K.; Chung, V. C.; Cheung, Y. T. *PLoS One* **2021**, *16* (7), No. e0253890.
(26) Gunalan, E.; Cebioglu, I. K.; Conak, O. *Complement Ther Med.* **2021**, *58*, 102682.
(27) *FTC, DOJ, and FDA Take Action to Stop Marketer of Herbal Tea from Making False COVID-19 Treatment Claims*; Federal Trade Commission, 2022.
(28) *FDA, WARNING LETTER: Tonic Therapeutic Herb Shop & Elixir Bar*; Federal Trade Commission, 2020.
(29) Zhang, Y.; Qi, D.; Gao, Y.; Liang, C.; Zhang, Y.; Ma, Z.; Liu, Y.; Peng, H.; Zhang, Y.; Qin, H.; Song, X.; Sun, X.; Li, Y.; Liu, Z. *J. Ethnopharmacol* **2020**, *260*, 112995.
(30) Caesar, L. K.; Cech, N. B. *Nat. Prod Rep* **2019**, *36* (6), 869−888.
(31) Kurita, K. L.; Glassey, E.; Linington, R. G. *Proceedings-of-the-national-academy-of-sciences-of-the-united-states Of-america.* **2015**, *112* (39), 11999−2004.
(32) Kellogg, J. J.; Todd, D. A.; Egan, J. M.; Raja, H. A.; Oberlies, N. H.; Kvalheim, O. M.; Cech, N. B. *J. Nat. Prod* **2016**, *79* (2), 376−86.
(33) Caesar, L. K.; Kellogg, J. J.; Kvalheim, O. M.; Cech, N. B. *J. Nat. Prod* **2019**, *82* (3), 469−484.
(34) Lee, S.; van Santen, J. A.; Farzaneh, N.; Liu, D. Y.; Pye, C. R.; Baumeister, T. U. H.; Wong, W. R.; Linington, R. G. *ACS Cent Sci.* **2022**, *8* (2), 223−234.
(35) McMillan, E. A.; Kwon, G.; Clemenceau, J. R.; Fisher, K. W.; Vaden, R. M.; Shaikh, A. F.; Neilsen, B. K.; Kelly, D.; Potts, M. B.; Sung, Y. J.; Mendiratta, S.; Hight, S. K.; Lee, Y.; MacMillan, J. B.; Lewis, R. E.; Kim, H. S.; White, M. A. *Cell Chem. Biol.* **2019**, *26* (10), 1380−1392.
(36) Potts, M. B.; Kim, H. S.; Fisher, K. W.; Hu, Y.; Carrasco, Y. P.; Bulut, G. B.; Ou, Y. H.; Herrera-Herrera, M. L.; Cubillos, F.; Mendiratta, S.; Xiao, G.; Hofree, M.; Ideker, T.; Xie, Y.; Huang, L. J.; Lewis, R. E.; MacMillan, J. B.; White, M. A. *Sci. Signal* **2013**, *6* (297), ra90.
(37) Neerukonda, S. N.; Vassell, R.; Herrup, R.; Liu, S.; Wang, T.; Takeda, K.; Yang, Y.; Lin, T. L.; Wang, W.; Weiss, C. D. *PLoS One* **2021**, *16* (3), No. e0248348.
(38) Hoffmann, M.; Kleine-Weber, H.; Schroeder, S.; Kruger, N.; Herrler, T.; Erichsen, S.; Schiergens, T. S.; Herrler, G.; Wu, N. H.; Nitsche, A.; Muller, M. A.; Drosten, C.; Pohlmann, S. *Cell* **2020**, *181*, 271.
(39) Beigel, J. H.; Tomashek, K. M.; Dodd, L. E.; Mehta, A. K.; Zingman, B. S.; Kalil, A. C.; Hohmann, E.; Chu, H. Y.; Luetkemeyer, A.; Kline, S.; Lopez de Castilla, D.; Finberg, R. W.; Dierberg, K.; Tapson, V.; Hsieh, L.; Patterson, T. F.; Paredes, R.; Sweeney, D. A.; Short, W. R.; Touloumi, G.; Lye, D. C.; Ohmagari, N.; Oh, M. D.; Ruiz-Palacios, G. M.; Benfield, T.; Fatkenheuer, G.; Kortepeter, M. G.; Atmar, R. L.; Creech, C. B.; Lundgren, J.; Babiker, A. G.; Pett, S.; Neaton, J. D.; Burgess, T. H.; Bonnett, T.; Green, M.; Makowski, M.; Osinusi, A.; Nayak, S.; Lane, H. C.; Members, A.-S. G. *New-england-journal-of-medicine.* **2020**, *383* (19), 1813−1826.
(40) Kellogg, J. J.; Paine, M. F.; McCune, J. S.; Oberlies, N. H.; Cech, N. B. *Nat. Prod Rep* **2019**, *36* (8), 1196−1221.
(41) Kim, D. E.; Min, J. S.; Jang, M. S.; Lee, J. Y.; Shin, Y. S.; Song, J. H.; Kim, H. R.; Kim, S.; Jin, Y. H.; Kwon, S. *Biomolecules* **2019**, *9* (11), 696.
(42) Halliwell, W. H. *Toxicol Pathol* **1997**, *25* (1), 53−60.
(43) Tummino, T. A.; Rezelj, V. V.; Fischer, B.; Fischer, A.; O'Meara, M. J.; Monel, B.; Vallet, T.; White, K. M.; Zhang, Z.; Alon, A.; Schadt, H.; O'Donnell, H. R.; Lyu, J.; Rosales, R.; McGovern, B. L.; Rathnasinghe, R.; Jangra, S.; Schotsaert, M.; Galarneau, J. R.; Krogan, N. J.; Urban, L.; Shokat, K. M.; Kruse, A. C.; Garcia-Sastre, A.; Schwartz, O.; Moretti, F.; Vignuzzi, M.; Pognan, F.; Shoichet, B. K. *Science* **2021**, *373* (6554), 541−547.
(44) Bhattacharyya, S., Inflammation During Virus Infection: Swings and Roundabouts. In *Dynamics of Immune Activation in Viral Diseases*; Bramhachari, P. V., Ed.; Springer Singapore: Singapore, 2020; pp 43−59.
(45) Sakurai, Y.; Kolokoltsov, A. A.; Chen, C. C.; Tidwell, M. W.; Bauta, W. E.; Klugbauer, N.; Grimm, C.; Wahl-Schott, C.; Biel, M.; Davey, R. A. *Science* **2015**, *347* (6225), 995−8.
(46) Du, X.; Zuo, X.; Meng, F.; Wu, F.; Zhao, X.; Li, C.; Cheng, G.; Qin, F. X. Combinatorial screening of a panel of FDA-approved drugs identifies several candidates with anti-Ebola activities. *Biochemical-and-biophysical-research-communications* **2020**, *522*, 862.
(47) Riva, L.; Yuan, S.; Yin, X.; Martin-Sancho, L.; Matsunaga, N.; Pache, L.; Burgstaller-Muehlbacher, S.; De Jesus, P. D.; Teriete, P.; Hull, M. V.; Chang, M. W.; Chan, J. F.; Cao, J.; Poon, V. K.; Herbert, K. M.; Cheng, K.; Nguyen, T. H.; Rubanov, A.; Pu, Y.; Nguyen, C.; Choi, A.; Rathnasinghe, R.; Schotsaert, M.; Miorin, L.; Dejosez, M.; Zwaka, T. P.; Sit, K. Y.; Martinez-Sobrido, L.; Liu, W. C.; White, K. M.; Chapman, M. E.; Lendy, E. K.; Glynne, R. J.; Albrecht, R.; Ruppin, E.; Mesecar, A. D.; Johnson, J. R.; Benner, C.; Sun, R.; Schultz, P. G.; Su, A. I.; Garcia-Sastre, A.; Chatterjee, A. K.; Yuen, K. Y.; Chanda, S. K. *Nature* **2020**, *586* (7827), 113−119.
(48) Jeon, S.; Ko, M.; Lee, J.; Choi, I.; Byun, S. Y.; Park, S.; Shum, D.; Kim, S. *Antimicrob. Agents Chemother.* **2020**, *64* (7), No. e00819-20.
(49) Gunaratne, G. S.; Yang, Y.; Li, F.; Walseth, T. F.; Marchant, J. S. *Cell Calcium* **2018**, *75*, 30−41.
(50) Luan, F.; He, X.; Zeng, N. *J. Pharm. Pharmacol* **2020**, *72* (11), 1491−1512.
(51) Herring, S.; Oda, J. M.; Wagoner, J.; Kirchmeier, D.; O'Connor, A.; Nelson, E. A.; Huang, Q.; Liang, Y.; DeWald, L. E.; Johansen, L. M.; Glass, P. J.; Olinger, G. G.; Ianevski, A.; Aittokallio, T.; Paine, M. F.; Fink, S. L.; White, J. M.; Polyak, S. J. *Antimicrob. Agents Chemother.* **2021**, *65* (4), No. e01146-20.
(52) Wagoner, J.; Herring, S.; Hsiang, T. Y.; Ianevski, A.; Biering, S. B.; Xu, S.; Hoffmann, M.; Pohlmann, S.; Gale, M.; Aittokallio, T.; Schiffer, J. T.; White, J. M.; Polyak, S. J. *Microbiol. Spectr.* **2022**, *10* (5), No. e0333122.
(53) Dobson, S. J.; Mankouri, J.; Whitehouse, A. *Antiviral-research.* **2020**, *179*, 104819.

https://doi.org/10.1021/acs.jnatprod.3c00159
J. Nat. Prod. 2023, 86, 1061−1073

(54) Chambers, M. C.; Maclean, B.; Burke, R.; Amodei, D.; Ruderman, D. L.; Neumann, S.; Gatto, L.; Fischer, B.; Pratt, B.; Egertson, J.; Hoff, K.; Kessner, D.; Tasman, N.; Shulman, N.; Frewen, B.; Baker, T. A.; Brusniak, M. Y.; Paulse, C.; Creasy, D.; Flashner, L.; Kani, K.; Moulding, C.; Seymour, S. L.; Nuwaysir, L. M.; Lefebvre, B.; Kuhlmann, F.; Roark, J.; Rainer, P.; Detlev, S.; Hemenway, T.; Huhmer, A.; Langridge, J.; Connolly, B.; Chadick, T.; Holly, K.; Eckels, J.; Deutsch, E. W.; Moritz, R. L.; Katz, J. E.; Agus, D. B.; MacCoss, M.; Tabb, D. L.; Mallick, P. *Nat. Biotechnol.* **2012**, *30* (10), 918−20.
(55) Pluskal, T.; Castillo, S.; Villar-Briones, A.; Oresic, M. *BMC Bioinformatics* **2010**, *11*, 395.
(56) Chau, F. T.; Chan, H. Y.; Cheung, C. Y.; Xu, C. J.; Liang, Y.; Kvalheim, O. M. *Anal. Chem.* **2009**, *81* (17), 7217−25.
(57) Rajalahti, T.; Kvalheim, O. M. *Int. J. Pharm.* **2011**, *417* (1−2), 280−90.
(58) Kvalheim, O. M.; Arneberg, R.; Bleie, O.; Rajalahti, T.; Smilde, A. K.; Westerhuis, J. A. *Journal of Chemometrics* **2014**, *28* (8), 615−622.
(59) Kvalheim, O. M. *Journal of Chemometrics* **2020**, *34* (4), No. e3211.
(60) Petit, C.; Bujard, A.; Skalicka-Wozniak, K.; Cretton, S.; Houriet, J.; Christen, P.; Carrupt, P. A.; Wolfender, J. L. *Planta Med.* **2016**, *82* (5), 424−31.
(61) Ritchie, M. E.; Phipson, B.; Wu, D.; Hu, Y.; Law, C. W.; Shi, W.; Smyth, G. K. *Nucleic Acids Res.* **2015**, *43* (7), No. e47-e47.
(62) Bateman, A.; et al. *Nucleic Acids Res.* **2023**, *51* (D1), D523−D531.
(63) Gaulton, A.; Hersey, A.; Nowotka, M.; Bento, A. P.; Chambers, J.; Mendez, D.; Mutowo, P.; Atkinson, F.; Bellis, L. J.; Cibrián-Uhalte, E.; Davies, M.; Dedman, N.; Karlsson, A.; Magariños, M. P.; Overington, J. P.; Papadatos, G.; Smit, I.; Leach, A. R. *Nucleic Acids Res.* **2017**, *45* (D1), D945−D954.
(64) Yu, G.; Wang, L. G.; Han, Y.; He, Q. Y. *OMICS* **2012**, *16* (5), 284−7.
(65) Wu, T.; Hu, E.; Xu, S.; Chen, M.; Guo, P.; Dai, Z.; Feng, T.; Zhou, L.; Tang, W.; Zhan, L.; Fu, X.; Liu, S.; Bo, X.; Yu, G. *Innovation (Camb)* **2021**, *2* (3), 100141.

https://doi.org/10.1021/acs.jnatprod.3c00159
J. Nat. Prod. 2023, 86, 1061−1073